Frictionless contact problem for hyperelastic materials with interior point optimizer

Houssam Houssein, Simon Garnotel, Frédéric Hecht

Frictionless contact problem for hyperelastic materials with interior point optimizer

Houssam Houssein[1,2], Simon Garnotel[2], Frédéric Hecht[1]

houssein@ljll.math.upmc.fr

simon.garnotel@airthium.com

frederic.hecht@sorbonne-universite.fr

[1] Sorbonne Université, CNRS, Université de Paris, Inria (Alpines), Laboratoire Jacques-Louis Lions (LJLL), F-75005 Paris, France.

[2]Airthium SAS, Accelair, 1 chemin de la Porte des Loges, 78350, Les Loges-en-Josas, France.

This work was partially funded by the "Association Nationale de la Recherche et de la Technologie" (ANRT)

Abstract

This paper presents a method to solve the mechanical problems undergoing finite deformations and the unilateral contact problems without friction for hyperelastic materials. We apply it to an industrial application: contact between a mechanical gasket and an obstacle. The main idea is to formulate the contact problem into an optimization's one, in order to use the Interior Point OPTimizer (IPOPT) to solve it. Finally, the FreeFEM software is used to compute and solve the contact problem. Our method is validated against several benchmarks and used on an industrial application example.

Keywords 1 *Contact, Frictionless, IPOPT, Interior point, Hertz, Unilateral*

1 Introduction

Mechanical contact problems and their simulations are of great importance in the industry. One of the difficulties encountered in these kinds of problems is the nonlinearity resulting from the non-penetration between the bodies coming into contact. Another nonlinearity can come from the material, indeed linear elastic materials are not used in practice to model the materials which can be submitted to large deformations, instead hyperelastic materials are considered to model materials like rubber. Hyperelastic materials mechanics are treated in [1, 5, 7, 15, 16].

Several formulations exist for contact problems, we can cite the primal formulation where the unknown is the displacement field or the dual formulation

where the contact pressure is the unknown of the problem. In this paper, we follow the contact primal formulation. Different methods can be used to solve a contact problem, like the penalty method, the Lagrangian multiplier method, and the augmented Lagrangian method. For more details about contact mechanics and methods that can be used for solving the problem, one can refer to the monographs [12, 22] and the references therein.

In [23], the penalty method was considered for a contact between a hyperelastic material and a rigid obstacle, the surface of the rigid obstacle was described by a C^2 function that can be given analytically or by cubic spline interpolation. Mixed formulations are used for example in [9, 10] where the unknowns are the displacement field and the contact pressure. A linear elasticity law is used to model the material and an Active Set Strategy was used in [10] in order to find the contact zone. In [17], an algorithm for contact problems involving fluid-structure interactions is presented and uses the semi-smooth Newton method. Several methods can be found in [24], like the Partial Dirichlet-Neumann method for unilateral contact. A barrier method was used in [13] to solve the contact problem.

In this paper, we restrict ourselves to the contact between a hyperelastic body (where the linear elastic body is a particular case) and a rigid obstacle or a rigid foundation. The dynamical and frictional cases are not treated here. The goal of this work is to propose a method that uses the FreeFEM software [8] and its tools to solve the contact problem. As it is formulated as an optimization problem, the Interior Point OPTimizer algorithm (IPOPT) [21], which is already interfaced with FreeFEM [8], is used to solve the optimization problem and to reach the solution. The rigid foundation is supposed to be described by a C^2 function, if it is not the case the foundation can be approximated by a spline function which is also available in the FreeFEM language.

This paper is organized as follows: in section 2, we present several reminders about large deformation mechanics and all useful quantities required to introduce our contact method, as well as the hyperelastic materials and the formulation of the contact problem between a body and a rigid foundation. In section 3, we present the Interior Point OPTimizer method (IPOPT), used to solve constrained minimization problems. We also introduce the formulation of our contact problem to be solved. Finally, in section 4, our method is validated against several contact examples and, in section 5, used in an industrial application.

2 Nonlinear mechanics

2.1 Large deformation mechanics

Let $\Omega \subset \mathbb{R}^3$ denotes a body and $\partial\Omega = \Gamma_0 \cup \Gamma_1$ where Γ_0 and Γ_1 denote respectively the disjoint parts of the boundary ($\Gamma_0 \cap \Gamma_1 = \emptyset$) where a displacement and a surface traction $\mathbf{t}$ are applied. Assuming the static case, the application which describes the deformation of the body is called Φ. It transforms the body

from its initial configuration Ω into its actual configuration $\Phi(\Omega)$, see Figure 1.

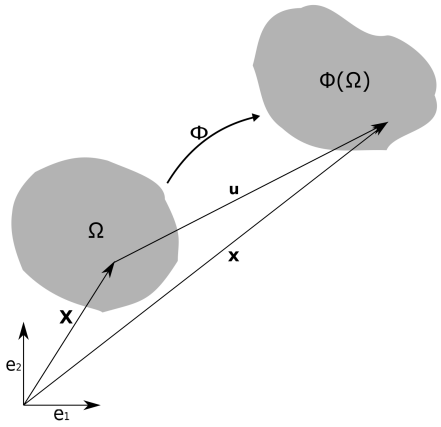

Figure 1: Initial and actual configurations.

In the following, the position vector of a particle in its initial and actual configuration is respectively represented by $\mathbf{X}$ and $\mathbf{x} = \Phi(\mathbf{X})$. The displacement field vector is given by:

$$\mathbf{u} = \mathbf{x} - \mathbf{X} = \Phi(\mathbf{X}) - \mathbf{X} \tag{1}$$

The deformation gradient $\mathbf{F}$ is a tensor that describes the deformation and is given by:

$$\mathbf{F} = \left(\frac{\partial \mathbf{x}}{\partial \mathbf{X}}\right)^T = \left(\frac{\partial \Phi(\mathbf{X})}{\partial \mathbf{X}}\right)^T \tag{2}$$

In a matrix form:

$$\mathbf{F}_{ij} = \frac{\partial \Phi_i}{\partial X_j} \tag{3}$$

Where $i, j \in \{1, 2, 3\}$. In addition, we have $det(\mathbf{F}) > 0$.

Moreover the right Cauchy-Green deformation tensor is defined by:

$$\mathbf{C} = \mathbf{F}^T.\mathbf{F} \tag{4}$$

There are three different types of tensors describing the stress in the body:

- Let ds, $\mathbf{n}$ denote respectively an infinitesimal surface in the body and the unitary normal vector at this surface (see Figure 2) in the actual configuration, thus the Cauchy stress tensor σ provides the force $d\mathbf{f}$ applied on ds by the following formula:

$$d\mathbf{f} = (\sigma.\mathbf{n})ds \tag{5}$$

- Let dS be the infinitesimal surface in the initial configuration, which corresponds to the surface ds in the actual configuration, and let $\mathbf{N}$ be the unitary

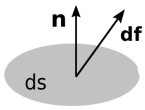

Figure 2: Infinitesimal surface.

normal vector at dS. Therefore the force $d\mathbf{f}$ in the actual configuration can also be given by:

$$d\mathbf{f} = (\mathbf{P}.\mathbf{N})dS \tag{6}$$

Where $\mathbf{P}$ denotes the first Piola-Kirchhoff stress tensor and can be obtained by the following:

$$\mathbf{P} = J\sigma\mathbf{F}^{-T} \tag{7}$$

And $J = det(\mathbf{F})$.

- Finally, the force applied at dS in the initial configuration denoted by $d\mathbf{F}$ can be provided by the following equation:

$$dF = (\mathbf{S}.\mathbf{N})dS \tag{8}$$

$\mathbf{S} = \mathbf{F}^{-1}\mathbf{P}$ denotes the Second Piola-Kirchhoff stress tensor. For more details one can refer to [18].

Let ρ be the actual density of the body, $\mathbf{f}$ the body force per unit mass applied on the body (for example the gravity), then the local balance of momentum in the actual configuration, where the Cauchy stress tensor is taken into account, is described by the following equation:

$$\text{div}(\sigma) + \rho\mathbf{f} = 0 \tag{9}$$

Or, by considering the components, it becomes:

$$\sum_{j=1}^{3} \frac{\partial \sigma_{ij}}{\partial x_j} + \rho f_i = 0 \quad i = 1, 2, 3 \tag{10}$$

The Cauchy stress tensor is symmetric ($\sigma = \sigma^T$) by the local balance of angular momentum. Note that in the reference configuration the local balance of momentum for the body can also be described by:

$$\sum_{j=1}^{3} \frac{\partial \mathbf{P}_{ij}}{\partial X_j} + \rho_0 f_i = 0 \quad i = 1, 2, 3 \tag{11}$$

Where ρ_0 is the body density in the reference configuration. In addition, boundary conditions must be imposed on the body boundary, therefore if we suppose a null displacement on Γ_0 and a surface traction $\mathbf{t}$ applied on Γ_1, we have the following conditions:

$$\begin{cases} \mathbf{u} & = \mathbf{0} \quad \text{on} \quad \Gamma_0 \\ \mathbf{P}.\mathbf{N} & = \mathbf{t} \quad \text{on} \quad \Gamma_1 \end{cases} \tag{12}$$

In the following, the admissible displacements set is defined by:

$$\mathcal{A} = \left\{ \mathbf{v} \in \left(H^1(\Omega)\right)^3 \ ; \ \mathbf{v} = 0 \text{ on } \Gamma_0 \right\} \tag{13}$$

Where $H^1(\Omega) = W^{1,2}(\Omega)$ is the Sobolev space. For more details on Sobolev spaces, one can refer to [3, 6].

The weak formulation in the initial configuration is the following:

$$\int_\Omega \mathbf{P} : Grad\, \mathbf{v}\, dV - \int_\Omega \rho_0 \mathbf{f}.\mathbf{v}\, dV - \int_{\Gamma_1} \mathbf{t}.\mathbf{v}\, dA = 0 \quad \forall\, \mathbf{v} \in \mathcal{A} \tag{14}$$

Where $(Grad\, \mathbf{v})_{ij} = \frac{\partial \mathbf{v}_i}{\partial X_j}$ and $A : B = tr(A^T B)$.

2.2 Hyperelastic materials

Hyperelastic materials describe a group of materials that can be subject to large deformations, for example rubber material.

In order to describe the behavior of a material supposed to be isotropic, the strain energy function Ψ provides a relation between the stress tensors and the displacement field, thus the second Piola-Kirchhoff stress tensor can be given by the following formula:

$$\mathbf{S} = 2.\frac{\partial \Psi}{\partial \mathbf{C}} \tag{15}$$

Or more explicitly by:

$$\mathbf{S}_{ij} = 2.\frac{\partial \Psi}{\partial \mathbf{C}_{ij}} \tag{16}$$

Where the tensor $\mathbf{C}$ is presented by the equation (4), and the strain energy function Ψ depends on the invariants (I_1, I_2, I_3) of the tensor $\mathbf{C}$:

$$\begin{cases} I_1 = tr(\mathbf{C}) \\ I_2 = \frac{1}{2}((tr(\mathbf{C}))^2 - tr(\mathbf{C}^2)) \\ I_3 = det(\mathbf{C}) = J^2 \end{cases} \tag{17}$$

We can cite for example two hyperelastic models: the Neo-Hookean and the Mooney models. The strain energy functions Ψ of these two models are given by:

$$\begin{cases} \Psi(I_1) = c_1(I_1 - 3) \quad \text{Neo-Hookean model} \\ \Psi(I_1, I_2) = c_2(I_1 - 3) + c_3(I_2 - 3) \quad \text{Mooney model} \end{cases} \tag{18}$$

Where c_1, c_2 and c_3 are material parameters.

The displacement field $\mathbf{u}$, solution of the equation (14), minimizes the total potential energy $\mathcal{E}$ over all admissible displacements. The total potential energy is defined by:

$$\mathcal{E}(\mathbf{v}) = \int_\Omega \Psi\, dV - \int_\Omega \rho_0 \mathbf{f}.\mathbf{v}\, dV - \int_{\Gamma_1} \mathbf{t}.\mathbf{v}\, dA \tag{19}$$

Therefore

$$\mathbf{u} = \underset{\mathbf{v}\in\mathcal{A}}{\operatorname{argmin}}(\mathcal{E}(\mathbf{v})) \tag{20}$$

Note that the weak formulation (14) presented above can be obtained from the minimization problem (20), indeed it can be done by taking the directional derivative of the energy $\mathcal{E}$ to be equal to zero:

$$D\mathcal{E}(u)(v) = 0 \quad \forall\, v \in \mathcal{A} \tag{21}$$

2.3 Signorini's contact problem

Signorini's contact problem [19] represents the contact between a deformable body and a fixed rigid foundation. An example is shown in Figure 3. Let $\Omega \subset \mathbb{R}^3$ denotes the body in its reference configuration, Γ_0 a part of the boundary $\partial\Omega$ where a displacement is imposed, $\Gamma_1 \subset \partial\Omega$ where the load is imposed, $\Gamma_2 \subset \partial\Omega$ the potential contact part of the boundary $\partial\Omega$. We also suppose that $\Gamma_0, \Gamma_1, \Gamma_2$ are disjoint and $\partial\Omega = \Gamma_0 \cup \Gamma_1 \cup \Gamma_2$ where Γ_2 has a non null area.

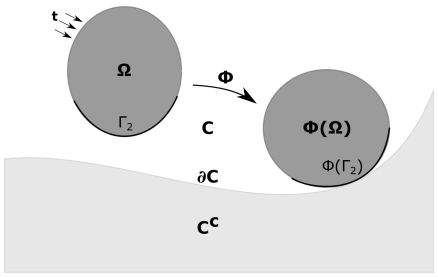

Figure 3: Signorini's contact.

Let $C \in \mathbb{R}^3$ be a closed set in $\mathbb{R}^3$, the complement of C describes the foundation where there is no penetration. The Signorini's contact equations are the set of the local balance of momentum equation, of the boundary and contact conditions. Using the same notations as before, the equations in the reference configuration are:

$$\begin{cases} \sum_{j=1}^{3} \frac{\partial \mathbf{P}_{ij}}{\partial X_j} + \rho_0 f_i = 0 \quad \text{in}\,\Omega \quad (i = 1, 2, 3) \\ \mathbf{u} = \mathbf{0} \quad \text{on} \quad \Gamma_0 \\ \mathbf{P}.\mathbf{N} = \mathbf{t} \quad \text{on} \quad \Gamma_1 \end{cases} \tag{22}$$

With the following contact conditions:

$$\begin{cases} \phi(\Gamma_2) \subset C \quad \text{(Non-penetration in the foundation)} \\ P.\mathbf{N} = 0 \quad \text{if}\, X \in \Gamma_2 \,\text{and}\, x = \phi(X) \in \text{int}(C) \\ P.\mathbf{N} = \lambda \mathbf{n} \quad \text{if}\, X \in \Gamma_2 \,\text{and}\, x = \phi(X) \in \partial C\,, \text{where}\, \lambda \leq 0 \end{cases} \tag{23}$$

For the hyperelastic materials, the first Piola-Kirchhoff stress tensor can be obtained by:

$$\mathbf{P} = \frac{\partial \Psi}{\partial \mathbf{F}} \tag{24}$$

The contact formulation described in (22) and (23) can be formulated like in [7] as a constrained minimization problem, i.e if $\mathbf{u}$ is the solution of Signorini's contact problem (22) and (23) then:

$$\mathbf{u} = \underset{v \in \mathcal{H}}{\operatorname{argmin}}(\mathcal{E}(v)) \tag{25}$$

Where $\mathcal{E}$ is the total potential energy defined in (19) and $\mathcal{H}$ is the set defined by:

$$\mathcal{H} = \left\{ \mathbf{v} \in \left(H^1(\Omega)\right)^3 \ ; \ \mathbf{v} = 0 \text{ on } \Gamma_0 \ ; \ \phi(\Gamma_2) \subset C \right\} \tag{26}$$

In many publications the normal gap function $g_n : \Gamma_2 \longrightarrow \mathbf{R}$ is used to describe the non-penetration condition: $\phi(\Gamma_2) \subset C$. The normal gap function g_n is a signed distance function between the body Ω and the foundation (see Figure 4). Let $\mathbf{x} \in \Phi(\Gamma_2)$ be a point of the deformed body $\Phi(\Omega)$, then the normal gap function is defined as the following:

$$g_n(\mathbf{x}) = (\mathbf{x} - \mathbf{y}).\mathbf{n}(\mathbf{y}) \tag{27}$$

Where $\mathbf{y}$ is the closest point of the rigid foundation to $\mathbf{x}$ and $\mathbf{n}(\mathbf{y})$ is the outward normal to the rigid foundation at $\mathbf{y}$. In this case the non-penetration condition is given by:

$$g_n(\mathbf{x}) \geq 0 \quad \forall \mathbf{x} \in \Phi(\Gamma_2) \tag{28}$$

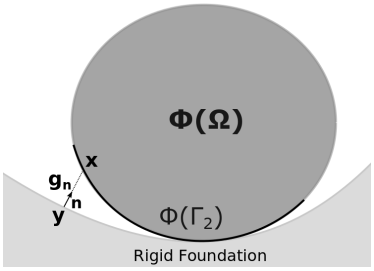

Figure 4: Normal gap function.

In other words, if $g_n(\mathbf{x}) > 0$ there is no penetration between the point $\mathbf{x}$ and the foundation, if $g_n(\mathbf{x}) = 0$ the point $\mathbf{x}$ and the foundation are in contact, finally if $g_n(\mathbf{x}) < 0$ the point $\mathbf{x}$ penetrates the foundation.

The non-penetration condition used in this paper is mentioned in the section 3.2.

3 Minimization problem resolution

3.1 Interior Point Optimizer

One of the open source software for optimization is IPOPT (Interior Point OPTimizer [21]). IPOPT can solve large scale constrained and unconstrained optimization problems where the constraints can be nonlinear. In other words, it solves the following problem:

$$\begin{cases} \underset{u\in\mathbb{R}^n}{Min}\, f(u) \quad \text{such that} \\ g_{Lo} \leq g(u) \leq g_{Up} \\ u_{Lo} \leq u \leq u_{Up} \end{cases} \tag{29}$$

Where $f : \mathbb{R}^n \to \mathbb{R}$ is the function to minimize and $g = (g^{(1)}, \ldots, g^{(m)}) : \mathbb{R}^n \to \mathbb{R}^m$ the inequality constraints. The two symbols Lo and Up denote respectively the lower and upper bounds, and the inequality between vectors means the inequality between the components of the vectors. In addition we suppose that $g_{Lo}^{(i)}, u_{Lo}^{(j)} \in \mathbb{R} \cup \{-\infty\}$ and finally $g_{Up}^{(i)}, u_{Up}^{(j)} \in \mathbb{R} \cup \{+\infty\}$ for all $i = 1, \ldots, m$ and $j = 1, \ldots, n$. The functions f and g are supposed to be sufficiently smooth (For example C^2).

By introducing the slack variables $s = (s^{(1)}, \ldots, s^{(m)}) \in \mathbb{R}^m$, the inequality constraint equations in (29) can be expressed as:

$$\begin{cases} g^{(i)}(u) - s^{(i)} = 0 \\ g_{Lo}^{(i)} \leq s^{(i)} \leq g_{Up}^{(i)} \quad \forall\, i = 1, \ldots, m \end{cases} \tag{30}$$

Therefore the minimization problem (29) is simplified and can thus be reformulated as follows:

$$\begin{cases} \underset{(u,s)\in\mathbb{R}^n\times\mathbb{R}^m}{Min}\, f(u) \quad \text{such that} \\ g(u) - s = 0 \\ (u_{Lo}, g_{Lo}) \leq (u, s) \leq (u_{Up}, g_{Up}) \end{cases} \tag{31}$$

Or in a simplified way and without loss of generality the problem can be transformed as follows:

$$\begin{cases} \underset{u\in\mathbb{R}^n}{Min}\, f(u) \quad \text{such that} \\ g(u) = 0 \\ u \geq 0 \end{cases} \tag{32}$$

IPOPT solves the minimization problem in multiple steps and we will only describe the principal ones, for more details see [20, 21]. The algorithm is briefly described in Algorithm 1:

The first-order optimality condition is given by:

$$\begin{cases} \nabla f(u) + \nabla g(u)\lambda - z = 0 \\ g(u) = 0 \\ UZe - \mu e = 0 \end{cases} \tag{33}$$

Algorithm 1 IPOPT

Define $\epsilon > 0$.
while the barrier parameter $\mu > \epsilon$ **do**
-The objective function f is transformed into a barrier function, and the problem is reformulated as follow:

$$\begin{cases} \underset{u \in \mathbb{R}^n}{Min}\, f(u) - \mu \sum_{i=1}^{n} ln(u^{(i)}) & \text{such that} \\ g(u) = 0 \end{cases}$$

while No convergence **do**
-First-order optimality condition for the barrier problem.
-Compute the descent directions $(d_k^u, d_k^\lambda, d_k^z)$ at the iteration k.
-Line search by filter method.
end while
-Decrease the barrier parameter μ.
end while
return $u \in \mathbb{R}^n$.

Where $\lambda \in \mathbb{R}^m$ and $z \in \mathbb{R}^n$ correspond respectively to the constraints and bounds Lagrange multipliers, $U = diag(u)$, $Z = diag(z)$ and finally where $e \in \mathbb{R}^n$ is a unit vector $e = (1, \ldots, 1)^T$.

A Newton method is applied to the system (33) in order to find the descent directions $(d_k^u, d_k^\lambda, d_k^z)$ at each iteration k. If u_k, λ_k, z_k denote respectively the values of u, λ, z at the iteration k, then the following system is obtained:

$$\begin{bmatrix} W_k & \nabla g(u_k) & -I_d \\ \nabla g(u_k)^T & 0 & 0 \\ Z_k & 0 & U_k \end{bmatrix} \begin{pmatrix} d_k^u \\ d_k^\lambda \\ d_k^z \end{pmatrix} = - \begin{pmatrix} \nabla f(u_k) + \nabla g(u_k)\lambda_k - z_k \\ g(u_k) \\ U_k Z_k e - \mu e \end{pmatrix} \tag{34}$$

Where $W_k = \nabla^2 \mathcal{L} = \nabla^2 f(u_k) + \sum_{j=1}^{m} \lambda_k^{(j)} \nabla^2 g^{(j)}(u_k)$, (j) denotes the components of a vector and $\mathcal{L}$ is the Lagrangian function.

Otherwise the linear system (34) can be reduced into the following:

$$\begin{bmatrix} W_k + U_k^{-1} Z_k & \nabla g(u_k) \\ \nabla g(u_k)^T & 0 \end{bmatrix} \begin{pmatrix} d_k^u \\ d_k^\lambda \end{pmatrix} = - \begin{pmatrix} \nabla \phi_\mu(u_k) + \nabla g(u_k)\lambda_k \\ g(u_k) \end{pmatrix} \tag{35}$$

with the additional equation:

$$d_k^z = \mu U_k^{-1} e - z_k - U_k^{-1} Z_k d_k^u \tag{36}$$

Where $\phi_\mu = f(u) - \mu \sum_{i=1}^{n} ln(u^i)$ is the barrier function.

As the descent direction was computed, the quantities $u_{k+1}, \lambda_{k+1}, z_{k+1}$ at the iteration k+1 are given by:

$$\begin{cases} u_{k+1} = u_k + \alpha_k d_k^u \\ \lambda_{k+1} = \lambda_k + \alpha_k d_k^\lambda \\ z_{k+1} = z_k + \alpha_k^z d_k^z \end{cases} \tag{37}$$

In order to improve the convergence of the algorithm, a linear search method with a filter method is used to determine the parameters α_k. Using the same notation as in [21], let $\theta(u) = \|g(u)\|$ be the constraint violation. At first a parameter α_k is proposed, a filter $\mathcal{F}$ is a set of $\mathbb{R}^2$, it helps to determine if α_k can be accepted as a step size and to avoid cycling between two successive solutions. Indeed when the optimization starts the filter is initialized as follow:

$$\mathcal{F}_0 = \{(\theta, \phi) \in \mathbb{R}^2 \,|\, \theta \geq \theta^{max}\} \tag{38}$$

Where θ^{max} is a chosen value. After each iteration the filter is updated according to the situation, to:

$$\mathcal{F}_{k+1} = \mathcal{F}_k \cup \{(\theta, \phi) \in \mathbb{R}^2 \,|\, \theta \geq (1 - \gamma_\theta)\theta(u_k) \;\&\; \phi \geq \phi_\mu(u_k) - \gamma_\phi \theta(u_k)\} \tag{39}$$

or to:

$$\mathcal{F}_{k+1} = \mathcal{F}_k \tag{40}$$

Where $(\gamma_\theta, \gamma_\phi) \in]0, 1[^2$ are two fixed values.

The step size α_k is accepted if $(\theta(u_{k+1}(\alpha_k)), \phi_\mu(u_{k+1}(\alpha_k))) \notin \mathcal{F}_k$, if it is not the case, several actions may be possible like the correction of the descent direction for example.

Finally the barrier parameter μ is decreased and the iteration starts from the last converged solution. The solution of the above algorithm, which depends on the barrier parameter $u(\mu)$, converges to the solution of the original problem (29) as $\mu \to 0$.

3.2 Formulation of the problem

In this section and without loss of generality we consider the two dimensional problem case. Using the same notations as section 2.3, let $\mathbf{X} = (X_1, X_2) \in \Gamma_2$ in the reference configuration, $\mathbf{x} = (x_1, x_2) \in \gamma_2 = \Phi(\Gamma_2)$ in the actual configuration and $\mathbf{u} = \mathbf{x} - \mathbf{X} = (u_1, u_2)$ its corresponding displacement vector, the non-penetration condition in our analysis will be written in the form of $\mathcal{S}(\mathbf{u}) \geq 0$, where $\mathcal{S} : \mathbb{R}^2 \longrightarrow \mathbb{R}$ is a function of class C^2.

We suppose that the boundary of the foundation can be written in the form of a function ψ (see Figure 5) of class C^2, then the non-penetration condition is given by:

$$x_2 - \psi(x_1) \geq 0 \tag{41}$$

This means that the body has to be always above the foundation in our case. By considering the reference configuration this condition becomes:

$$\mathcal{S}(\mathbf{u}) = X_2 + u_2 - \psi(X_1 + u_1) \geq 0 \tag{42}$$

If the function ψ of the foundation is not subject to a large variations then we can apply Taylor's theorem to $\psi(X_1 + u_1)$ and obtain a simpler non-penetration condition:

$$\mathcal{S}(\mathbf{u}) = X_2 - \psi(X_1) + u_2 - \psi'(X_1).u_1 \geq 0 \tag{43}$$

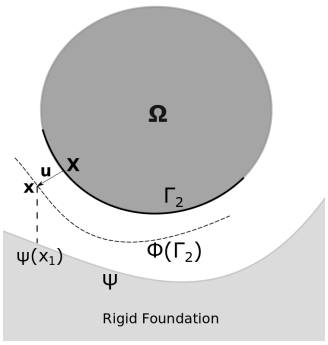

Figure 5: The foundation function ψ.

In finite element method, the body domain Ω can be approximated by a polygonal domain $\Omega_h = \bigcup_{i=1}^{n_T} T_i$ where T_i are the triangles which constitute Ω_h and h the mesh size. Let $\mathcal{T}_h$ be the family of the triangles T_i and without loss of generality let $V_h(P_1)$ be the linear finite element space defined on Ω_h and given by:

$$V_h(P_1, \mathcal{T}_h) = \left\{ v(x,y) = \sum_{k=1}^{m} v_k \Phi_k(x,y) \,|\, v_k \in \mathbb{R} \right\} \tag{44}$$

Where m denotes the number of nodes (or vertex) in the mesh and Φ_k the shape function which in our case is linear on each triangle and is equal to 1 at the node k and zero at the others nodes. The component v_k is called a degree of freedom of the function v, we note also that the function v is a continuous piecewise function.

In our analysis, we are interested to find the displacement field $\mathbf{u} = (u_x, u_y)$ for the unilateral contact problem. First we consider that $u_x\,, u_y \in V_h$, if $\{U_{x,1} \dots U_{x,m}\}$ and $\{U_{y,1} \dots U_{y,m}\}$ denote respectively the degrees of freedom of u_x and u_y, then the degrees of freedom of $\mathbf{u}$ are given by:

$$\mathbf{U} = \begin{pmatrix} U_1 \\ U_2 \\ \vdots \\ U_{n-1} \\ U_n \end{pmatrix} = \begin{pmatrix} U_{x,1} \\ U_{y,1} \\ \vdots \\ U_{x,m} \\ U_{y,m} \end{pmatrix} \tag{45}$$

Where $n = 2m$. The degrees of freedom $\mathbf{U}$ of the displacement field describe the nodes displacement of the mesh.

Our contact problem can be formulated as follow:

$$\begin{cases} \underset{\mathbf{U} \in \mathbb{R}^n}{Min}\, \mathcal{E}(\mathbf{U}) & \text{such that} \\ d(\mathbf{U}) \geq 0 \end{cases} \tag{46}$$

Where $\mathbf{U} \in \mathbb{R}^n$ is the displacement vector of the body mesh nodes, $\mathcal{E}(\mathbf{U})$ is the total potential energy of the body and finally $d = (d^{(1)}, \ldots, d^{(n_b)}) : \mathbb{R}^n \to \mathbb{R}^{n_b}$ represents the non-penetration condition with the rigid foundation for each node of the boundary (Γ_2) and n_b is the number of the boundary (Γ_2) nodes.

More precisely $d^{(i)}$ represents the non-penetration condition for the node i belonging to the boundary (Γ_2) and is defined by:

$$d^{(i)}(\mathbf{U}) = \mathcal{S}(D_{xi}, D_{yi}) \tag{47}$$

Where $\mathcal{S}$ is defined in (42) and (D_{xi}, D_{yi}) is the displacement vector for the node i.

Finally, we obtain a constrained minimization problem which can be solved by the Interior Point OPTimizer (IPOPT) as we will see in the next section.

4 Numerical validations

In this section, we present several common numerical examples in order to validate our method. First, we will present two tests in 2D and 3D on the compression of a hyperelastic cube with two specific types of materials. In these tests the contact is not taken into account, indeed the goal is to validate our algorithm in solving problems with a hyperelastic material behavior. Next, we present 3 contact tests, where 2 are a Hertz contact problem with an explicit analytic solutions, to validate our contact method for an arbitrary rigid foundation.

In FreeFEM, necessary quantities like the energy and the constraints (Jacobian, Hessian) are computed, then IPOPT is used to solve our constrained minimization problem through its FreeFEM interface. To see how we can use IPOPT with FreeFEM one can refer to [4, 8]. The advantage of this method is that we have just to formulate our contact problem and IPOPT will act like a black box to solve the optimization problem.

4.1 Compression of a hyperelastic cube

Here we handle the tests presented in [2]. A unit cube of dimension equal to $1\,m$ is considered (see Figure 6), the cube can move along the direction X_1 and its two faces which are perpendicular to the direction X_3 are fixed along this last direction, finally, the lower face of this cube is fixed along the direction X_2. A pressure of $f = 0.876\,Pa$ is applied on the upper face of the cube.

Two nearly incompressible hyperelastic material models [14] are considered for the cube: Neo-Hookean and Mooney. These models describe also the incompressibility of the two materials. The goal is to compute the displacement field (specifically the vertical displacement) and to compare it with the theoretical one. The strain energy functions of these two models are given as follow:

$$\psi = C_{10}(J^{-\frac{2}{3}} I_1 - 3) + C_{01}(J^{-\frac{4}{3}} I_2 - 3) + \frac{K}{2}(J-1)^2 \tag{48}$$

Where $K = \frac{6(C_{01}+C_{10})}{3(1-2\nu)}$ [14] and ν is the Poisson's ratio. The function $\frac{K}{2}(J-1)^2$ helps to satisfy the incompressibility constraint ($J = 1$) by penalizing it. The coefficients C_{01}, C_{10} and ν are presented in the table 1:

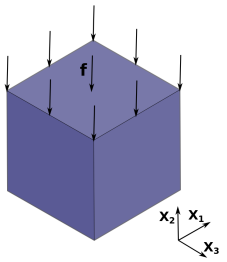

Figure 6: The cube with the applied pressure.

Table 1: Material coefficients

Coefficients	Mooney	Neo-Hookean
C_{10}	0.709	1.2345
C_{01}	2.3456	0.
ν	0.499	0.499

The linear finite element P_1 [8] was used for this study and the mesh contains 200 elements in the two dimensional case. In order to avoid the rigid movement of the structure and using the fact that the problem is symmetric, only half of the structure is modeled like we can see in Figure 7 for the two dimensional case.

Using IPOPT in order to minimize the total potential energy of the cube and generate the displacement field, the maximum vertical displacement of the upper face is given in the table 2.

FreeFEM in 2D	Mooney	Neo-Hookean
w	0.034072	0.078331

Table 2: Vertical displacement w with FreeFEM in 2D

The errors with respect to the theoretical values for our method and Code_Aster [2] are presented in the table 3 where we can see similar results.

In the Figure 8a, the deformed shape and the vertical displacement for the Neo-Hookean material case is shown. To see the FreeFEM script of the example presented above, please visit `https://modules.freefem.org/modules/nonlinear-elasticity/`.

On the other hand, the exact same results were generated by considering the three dimensional case for the two type of materials. In addition, note that we obtained the same results for the displacement field by supposing that the cube is in contact on its lower face with a rigid foundation, see Figure 8b for the three dimensional case.

4.2 Hertz contact problem

A classical contact problem is the contact between two deformable cylinders where their axis are parallel, and a theoretical solution exists for this type of

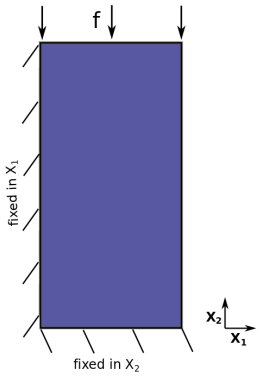

Figure 7: The 2D symmetrical model of the cube.

Table 3: Errors with respect to the theoretical values

Errors	FreeFEM	Code_Aster
Errors in 2D (Mooney)	0.19%	0.20%
Errors in 2D (Neo-Hookean)	0.19%	0.20%

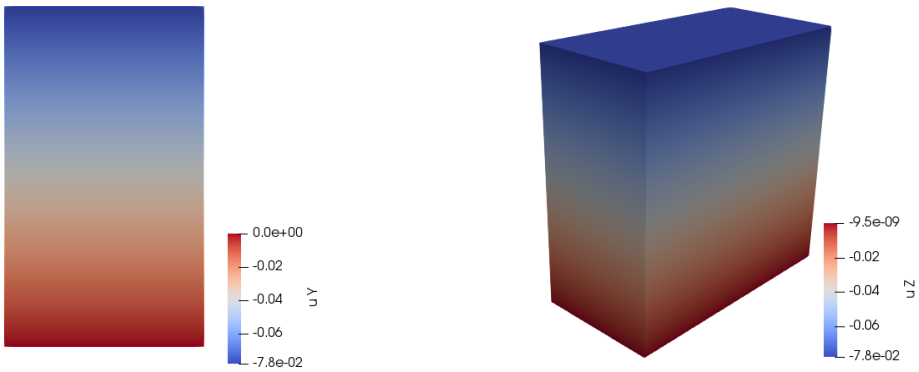

(a) 2D case (b) 3D case

Figure 8: Vertical displacement field (Neo-Hookean).

problems (see [11]). In the following, the plane strain situation is considered and it corresponds to the two dimensional case (2D). In other words, the height of the cylinders is large. Finally, the frictionless contact is also supposed.

In general, the zone of contact between the cylinders is a strip of width $2a$, in the 2D situation the contact becomes between two discs. The quantity of interest is the normal pressure at the contact zone. Let a force of magnitude P be applied on the first cylinder and let this force be normal to its axis in order to compress the two bodies and let them enter in contact. Therefore, by assuming the hypothesis of small deformations and linear elasticity we can obtain analytically the half length of the contact zone a in addition to the profile of the normal pressure at the contact zone.

Let R_1 and R_2 denote the radius of the cylinders, E_1, E_2 the Young's modulus and ν_1, ν_2 the Poisson's ratio of the first and second cylinder, then the half contact length a is given by:

$$a = \sqrt{\frac{4PR}{\pi E^*}} \tag{49}$$

Where R and E^* are computed as follow:

$$\begin{cases} \frac{1}{R} = \frac{1}{R_1} + \frac{1}{R_2} \\ \frac{1}{E^*} = \frac{1-\nu_1^2}{E_1} + \frac{1-\nu_2^2}{E_2} \end{cases} \tag{50}$$

Let x denotes the coordinate along the contact zone, thus the normal pressure profile p is given as follow:

$$p(x) = p_{max}\sqrt{1 - \frac{x^2}{a^2}} \tag{51}$$

Where $p_{max} = \frac{2P}{\pi a}$, the maximum pressure, is located at the origin of the contact zone.

The second cylinder can be considered as a rigid foundation by taking a large value of its Young's modulus $E_2 \to +\infty$, thus we obtain $E^* \to \frac{E_1}{1-\nu_1^2}$ and the same equations presented above can be used.

In the same manner, the second cylinder can be replaced by a plane by taking $R_2 \to +\infty$, therefore $R \to R_1$.

Next we present the numerical results of two contact examples involving a deformable cylinder against a rigid foundation. The foundation is respectively a plane and a cylinder for the first and second example. Due to the two dimensional case and the symmetry of the problem, only a quarter of a disc, which represents the cylinder, will be modeled. In the two examples f denotes the pressure applied on the top face of the quarter disc, R_1, E_1 and ν_1 denote respectively the radius, Young's modulus and the Poisson's ratio of the quarter disc. Note that the total force applied is equal to $P = 2fR_1$.

4.2.1 Contact with a rigid plane foundation

The contact between the quarter disc and the rigid plane is shown below (Figure 9a). In order to compare our results to the theoretical one, we suppose the following values: a radius $R_1 = 1\,m$, a Young's modulus $E_1 = 2.1 \times 10^9\,Pa$, a Poisson's ratio $\nu_1 = 0.3$ and finally a top face pressure of $f = 2.75 \times 10^6\,Pa$.

In this case the half contact length a is equal to:

$$a = \sqrt{\frac{8fR_1^2(1-\nu_1^2)}{\pi E_1}} \tag{52}$$

The maximum pressure and the pressure profile at the contact zone are equal to:

$$p_{max} = \frac{4fR_1}{\pi a} \tag{53}$$

$$p(x) = p_{max}\sqrt{1 - \frac{x^2}{a^2}} \tag{54}$$

The linear finite element P_1 was used for the simulation and the mesh was refined at the contact zone. In Figure 9b, we can see the deformation of the quarter disc in addition to the distribution of the Von Mises stress, and we also remark that the maximum Von Mises stress is not at the border where the contact occurs.

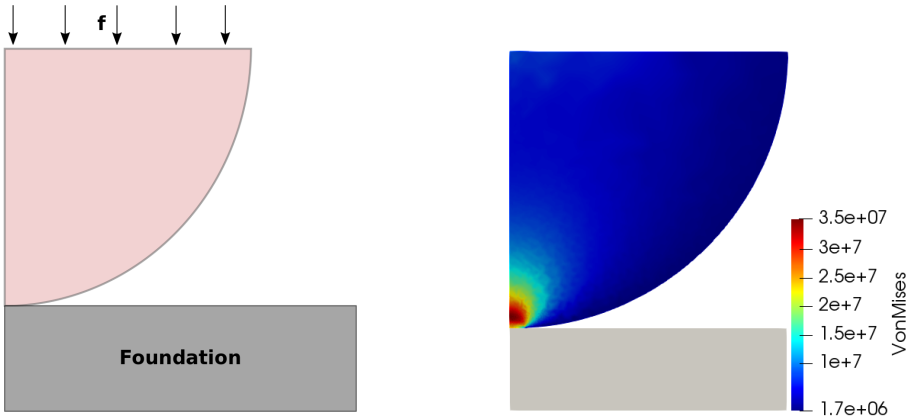

(a) The geometry

(b) Deformation and Von mises stress.

Figure 9: Contact with a rigid plane foundation.

The pressure at the contact zone $p(x)$ computed with our algorithm is plotted with the theoretical one in the Figure 10.

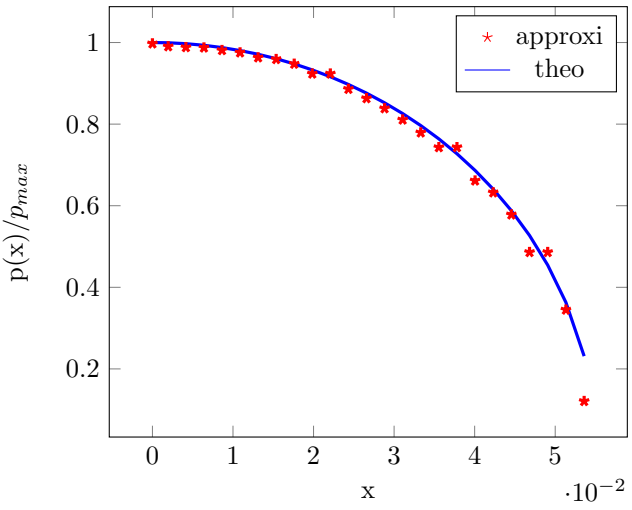

Figure 10: Pressure at the contact zone.

4.2.2 Contact with a rigid circular foundation

In this example the contact is between the quarter disc and a rigid cylinder of radius $R_2 = 1.2\,m$, also modeled by a quarter disc (Figure 11a). The properties of the deformable quarter disc are the following: a radius $R_1 = 1\,m$, Young's modulus $E_1 = 2.1 \times 10^5\,Pa$, and a Poisson's ratio $\nu_1 = 0.3$. The top face pressure is equal to $f = 250\,Pa$.

The half contact length a can be computed analytically by:

$$a = \sqrt{\frac{8fR_1R(1-\nu_1^2)}{\pi E_1}} \tag{55}$$

Where $R = \frac{R_1R_2}{R_1+R_2}$. Using the same formulas, the maximum pressure and the pressure profile at the contact zone are equal to:

$$p_{max} = \frac{4fR_1}{\pi a} \tag{56}$$

$$p(x) = p_{max}\sqrt{1-\frac{x^2}{a^2}} \tag{57}$$

Like the previous example the linear finite element P_1 was used for the simulation and the mesh was refined at the contact zone, moreover the rigid foundation was constructed with a spline function. The deformation of the quarter disc in addition to the distribution of the Von Mises stress are shown in the Figure 11b.

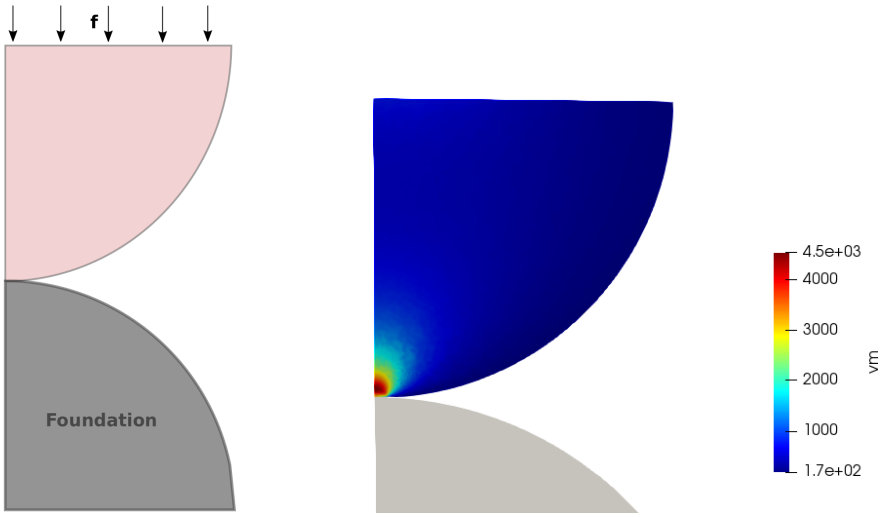

(a) The geometry

(b) Deformation and Von mises stress.

Figure 11: Contact with a rigid circular foundation.

The Figure 12 shows the computed pressure at the contact zone $p(x)$ with the theoretical one.

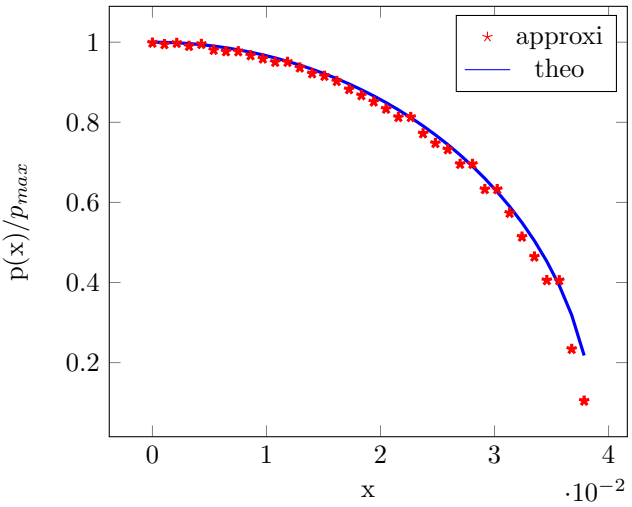

Figure 12: Pressure at the contact zone.

4.3 Clamped body contact

In this test an iron square Ω of length equal to $1\,m$ is considered, the square is clamped on its side Γ_0 and is initially in contact with a rigid plane on its side Γ_2 (see Figure 13a). The body is subjected by its own weight where $\rho = 7800\,kg.m^{-3}$ and $g = 9.81\,m.s^{-2}$. The properties of the elastic body are the Young's modulus $E = 2.1 \times 10^{11}\,Pa$ and the Poisson's ration $\nu = 0.3$. This test was treated in [9]. A uniform mesh was taken with 51 nodes at each side, the finite element used is the $P2$ element.

The deformed configuration of the body is shown in the Figure 13b with an amplification factor.

In Figure 14, the contact pressure on the left side Γ_2 is plotted in comparison with the values found in [9].

5 Industrial application example

In this analysis an O-ring gasket is trapped between two metallic parts (see Figure 15). As the radius of the gasket section is small compared to its circumference, we suppose that we are in the plane strain configuration, thus only a section of the gasket is studied. In this analysis the metallic parts are supposed to be rigid.

The following data are only used to illustrate the behavior of the gasket, thus a radius of $R = 0.52m$ is taken for the gasket section, the gap between the two supports is $g = 0.2m$, the material model considered for this simulation is the Neo-Hookean model presented in (48), and finally the inner shape of the two metallic parts is a square of dimension $l = 1m$.

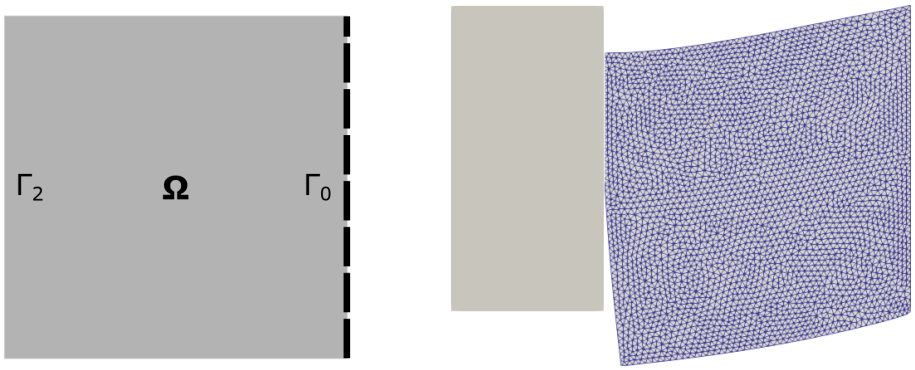

(a) The geometry

(b) The body deformation (amplification factor $= 2.10^5$).

Figure 13: The square iron problem.

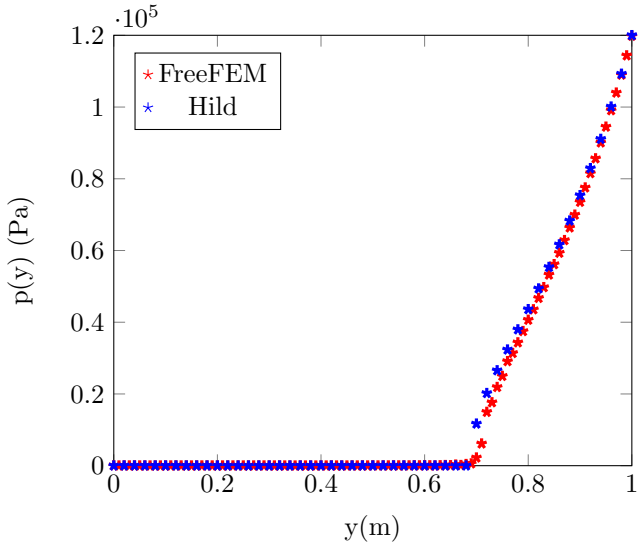

Figure 14: Contact pressure at the side Γ_2 of the body.

The deformed shape of the compressed gasket and the Von-mises stress distribution are shown in the Figure 16.

6 Conclusion

In this work, we formulated the unilateral frictionless contact problem into a constrained minimization problem and we used IPOPT like a black box to solve the optimization problem. The proposed method has the advantage of being

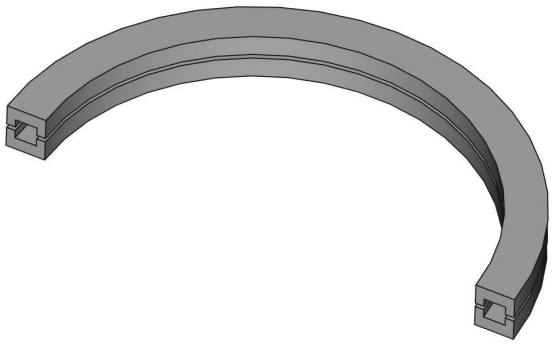

Figure 15: The two metallic parts where the gasket is trapped.

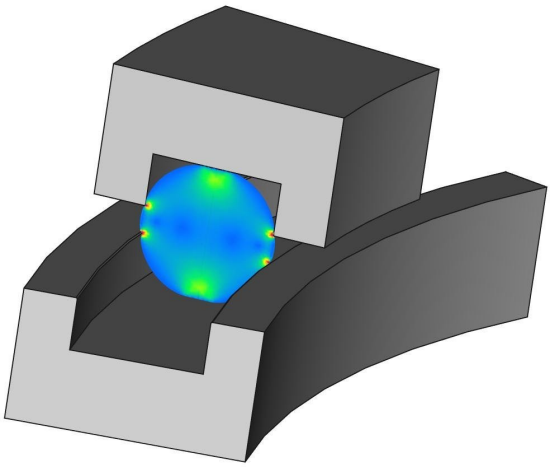

Figure 16: The deformed shape and the Von-mises stress distribution.

simple to implement in FreeFEM because optimization tools are already available. The results of the nonlinear behavior tests were similar to those obtained by Code_Aster, besides, as we showed in the validation section, our contact method gave results close to the analytic one or results done by other methods. In the future, the scope of the method will be extended to the contact between two bodies, and to the dynamic case.

Acknowledgments

We would like to acknowledge Franck Lahaye from , Airthium SAS, for his linguistic help.

References

[1] M. ABBAS, *Code_Aster [R5.03.19] Loi de comportement hyperélastique : matériau presque incompressible*, EDF R&D, 8 2013.

[2] M. ABBAS, *Code_Aster [V6.04.187] SSNV187 - Validation de la loi ELAS_HYPER sur un cube*, EDF R&D, 5 2018.

[3] R. A. Adams and J. J. Fournier, *Sobolev spaces*, vol. 140, Elsevier, 2003.

[4] S. Auliac, *développement d'outils d'optimisation pour freefem++*, PhD thesis, Université Pierre et Marie Curie-Paris VI, 2014.

[5] J. Bonet and R. D. Wood, *Nonlinear continuum mechanics for finite element analysis*, Cambridge university press, 1997.

[6] H. Brezis, *Functional analysis, Sobolev spaces and partial differential equations*, Springer Science & Business Media, 2010.

[7] P. G. Ciarlet, *Three-dimensional elasticity*, vol. 20, Elsevier, 1988.

[8] F. Hecht, *New development in freefem++*, J. Numer. Math., 20 (2012), pp. 251–265.

[9] P. Hild, *A sign preserving mixed finite element approximation for contact problems*, International Journal of Applied Mathematics and Computer Science, 21 (2011), pp. 487–498.

[10] S. Hüeber and B. I. Wohlmuth, *A primal–dual active set strategy for non-linear multibody contact problems*, Computer Methods in Applied Mechanics and Engineering, 194 (2005), pp. 3147–3166.

[11] K. L. Johnson, *Contact mechanics*, Cambridge university press, 1985.

[12] N. Kikuchi and J. T. Oden, *Contact problems in elasticity: a study of variational inequalities and finite element methods*, vol. 8, siam, 1988.

[13] G. Kloosterman, R. M. van Damme, A. H. van den Boogaard, and J. Huetink, *A geometrical-based contact algorithm using a barrier method*, International Journal for Numerical Methods in Engineering, 51 (2001), pp. 865–882.

[14] J.-P. LEFEBVRE, *Code_Aster [U4.43.01] Operator DEFI_MATERIAU*, EDF R&D, 7 2018.

[15] G. Marckmann and E. Verron, *Comparison of hyperelastic models for rubber-like materials*, Rubber chemistry and technology, 79 (2006), pp. 835–858.

[16] R. W. Ogden, *Large deformation isotropic elasticity–on the correlation of theory and experiment for incompressible rubberlike solids*, Proc. R. Soc. Lond. A, 326 (1972), pp. 565–584.

[17] O. Pironneau, *Handling contacts in an eulerian frame: a finite element approach for fluid structures with contacts*, International Journal of Computational Fluid Dynamics, 32 (2018), pp. 121–130.

[18] J. N. Reddy, *An introduction to continuum mechanics*, Cambridge university press, 2013.

[19] A. Signorini, *Sopra alcune questioni di elastostatica*, Atti della Societa Italiana per il Progresso delle Scienze, 21 (1933), pp. 143–148.

[20] A. Wächter, *Short tutorial: getting started with ipopt in 90 minutes*, in Dagstuhl Seminar Proceedings, Schloss Dagstuhl-Leibniz-Zentrum für Informatik, 2009.

[21] A. Wächter and L. T. Biegler, *On the implementation of an interior-point filter line-search algorithm for large-scale nonlinear programming*, Mathematical programming, 106 (2006), pp. 25–57.

[22] P. Wriggers, *Computational Contact Mechanics, Second Edition*, Springer-Verlag, 2006.

[23] P. Wriggers and M. Imhof, *On the treatment of nonlinear unilateral contact problems*, Archive of Applied Mechanics, 63 (1993), pp. 116–129.

[24] V. Yastrebov, *Computational contact mechanics: geometry, detection and numerical techniques*, PhD thesis, École Nationale Supérieure des Mines de Paris, 2011.